Research Square

Preprints are preliminary reports that have not undergone peer review.
They should not be considered conclusive, used to inform clinical practice,
or referenced by the media as validated information.

Design and Experimental Validation of an APSO-Optimized Fractional-Order PI Controller for a Single-Phase Boost Power Factor Correction Converter

Adel Ballouti
University of M'sila
Nouri Belhaouchet
University Ferhat Abbas of Setif
Salah AMROUNE
University of M'sila
Yassine Bensafia
University of Bouira
Eustache Hakizimana
haki2012eustache@gmail.com
University of Rwanda

Article

Keywords: Fractional-Order Proportional-Integral (FOPI), Adaptive Particle Swarm Optimization (APSO), Power Factor Correction (PFC), Single-Phase Boost Converter, Oustaloup Approximation, Tustin Transformation

Posted Date: November 25th, 2026

DOI: https://doi.org/10.21203/rs.3.rs-11691907/v1

License: This work is licensed under a Creative Commons Attribution 4.0 International License.
Read Full License

Additional Declarations: No competing interests reported.

Design and Experimental Validation of an APSO-Optimized Fractional-Order PI Controller for a Single-Phase Boost Power Factor Correction Converter

Adel Ballouti [1,2,*], Nouri Belhaouchet [2], Salah Amroune[3,4], Yassine Bensafia[5] , Eustache Hakizimana[6,*]

[1]*Electronic Department, Faculty of Technology, University of M'sila, University Pole, Road Bourdj Bou Arreiridj, M'sila 28000, Algeria.*
[2]*LAS Laboratory, Department of Electrical Engineering, Faculty of Technology, Setif 1 University-Ferhat Abbas, 19000 Setif, Algeria.*
[3]*Mechanical Engineering Department, Faculty of Technology, University of Msila, University Pole, Road Bourdj Bou Arreiridj, M'sila 28000, Algeria.*
[4]*Laboratory of Materials and Mechanics of Structures (LMMS), Faculty of technology, University of M'sila, University Pole, Road Bourdj Bou Arreiridj, M'sila 28000, Algeria*
[5] *LISEA Laboratory, Electrical Engineering Department, Faculty of Applied sciences, University of Bouira 10000 ,Algeria.*
[6]*University of Rwanda, Mechanical and Energy Engineering Department, PoBoX, 3900, Kigali, Rwanda.*

[*] Correspondence: adel.ballouti@univ-msila.dz ; haki2012eustache@gmail.com

Abstract— This paper presents the design and implementation of an Adaptive Particle Swarm Optimization (APSO)-optimized Fractional-Order Proportional-Integral (FOPI) controller for a single-phase AC–DC boost Power Factor Correction (PFC) converter. The optimization employs an Integral of Time-weighted Absolute Error (ITAE)-centered composite objective function incorporating Integral Absolute Error (IAE), overshoot, settling time, control effort, and control-signal variation. The inertia weight, cognitive coefficient, and social coefficient are adaptively varied throughout the optimization process to promote a progressive transition from global exploration to local exploitation. The fractional-order integrator is approximated using the Oustaloup method, and the resulting rational transfer function is subsequently discretized using the Tustin (bilinear) transformation for digital implementation. The proposed controller is evaluated in MATLAB/Simulink under steady-state and transient operating conditions and is subsequently implemented experimentally using a dSPACE 1104 real-time control system. The experimental results demonstrate a near-unity Power Factor (PF) of 0.997 and an input-current Total Harmonic Distortion (THD) of 4.3% under steady-state operation. For DC-link voltage reference variations, the FOPI controller achieves a settling time of approximately 50 ms in simulation and 60 ms experimentally. Under load-resistance variations, the experimental DC-link voltage deviation is limited to approximately 2 V, with recovery times of about 60 ms for the tested transitions. The results demonstrate that the APSO-optimized FOPI controller provides improved dynamic DC-link voltage regulation while maintaining satisfactory steady-state power-quality performance.

Keywords—Fractional-Order Proportional-Integral (FOPI), Adaptive Particle Swarm Optimization (APSO), Power Factor Correction (PFC), Single-Phase Boost Converter, Oustaloup Approximation, Tustin Transformation.

1. INTRODUCTION

The increasing use of power electronic converters in modern electrical systems has intensified concerns regarding power quality, particularly input-current harmonic distortion and poor power factor [1], [2]. Single-phase AC–DC converters based on conventional diode-bridge rectifiers draw highly distorted currents from the utility grid because the input current flows mainly around the peaks of the AC voltage waveform [2], [3]. Such current distortion increases harmonic pollution and reduces the effective utilization of the electrical supply [2]. Consequently, power factor correction (PFC) has become an important requirement in modern AC–DC conversion systems, particularly in applications where compliance with harmonic-current limits such as IEEE Std 519 [4–5] and high power factor are required [1]–[5].

Among the different PFC configurations, the single-phase boost PFC converter is widely used because of its relatively simple structure, continuous input-current characteristic, and ability to provide a regulated DC-link voltage while achieving near-unity power factor [6]–[8]. The conventional control structure generally consists of cascaded current and voltage control loops [6], [9]. The inner current loop shapes the input current according to a sinusoidal reference synchronized with the AC source voltage, whereas the outer voltage loop regulates the DC-link voltage and compensates for variations in the input power and load demand [1-3], [6-9]. The performance of the outer voltage controller therefore has a significant influence on the transient behavior of the converter.

Conventional Proportional-Integral (PI) controllers are widely used for DC-link voltage control owing to their simple structure and zero steady-state error [1-3], [6-9]. Nevertheless, relying on only two tuning parameters (Kp and Ki) limits their capacity to simultaneously optimize transient speed, overshoot, settling time, and parameter robustness under dynamic load variations. To overcome these constraints, advanced control strategies with expanded degrees of freedom have gained attention for PFC converter applications.

Fractional-order calculus extends conventional integer-order calculus by introducing non-integer differentiation and integration orders, thereby providing an additional degree of freedom for control-system design. In particular, the Fractional-Order Proportional-Integral (FOPI) controller introduces the fractional integration order λ in addition to the conventional proportional and integral gains [10], [12]. The FOPI controller can be expressed as:

$$G_{\mathrm{FOPI}}(s) = K_p + K_i.\frac{1}{s^{\lambda}}, \dots\dots\dots\dots\dots (1)$$

Where Kp and Ki denote the proportional and integral gains, respectively, and λ is the fractional integration order. The additional parameter λ provides greater flexibility in shaping the dynamic and frequency-domain characteristics of the closed-loop system and can therefore be exploited to improve transient performance and robustness [10-12].

Despite these advantages, an ideal fractional-order operator cannot generally be represented exactly by a finite-order rational transfer function. Practical implementation therefore requires an approximation of the fractional operator over a specified frequency range. Several approaches have been investigated for the numerical realization of fractional-order operators, including the frequency-domain rational approximation techniques [10-12] and Grünwald–Letnikov (GL) formulation [13].

While the GL formulation provides a direct time-domain representation, it requires a large memory buffer for history accumulation. Conversely, frequency-domain methods approximate the fractional operator using a finite number of poles and zeros [11], [12]. In this work, the Oustaloup recursive approximation is selected to approximate the fractional integrator $s^{-\lambda}$ over a predefined frequency range [14-17]. This approach provides a finite-order rational representation of the fractional operator, making it suitable for numerical simulation and subsequent digital implementation. The resulting rational approximation is subsequently discretized using the Tustin (bilinear) transformation to obtain the discrete-time controller representation required for real-time implementation [17-19].

The parameters of the FOPI controller (Kp, Ki, and λ) are coupled and directly affect tracking error, overshoot, response time, and control effort. Tuning these parameters simultaneously is more challenging than tuning conventional PI controller parameters. Traditional tuning methods—analytical or manual—may require considerable effort without guaranteeing satisfactory performance when multiple objectives must be satisfied at the same time. Optimization-based approaches offer a viable alternative by systematically exploring the controller parameter space according to predefined performance criteria.

Particle Swarm Optimization (PSO) [20-26] is a population-based optimization technique that has been widely applied to controller parameter tuning because of its relatively simple structure and ability to search nonlinear parameter spaces. In conventional PSO, the inertia weight and acceleration coefficients significantly influence the balance between global exploration and local exploitation. In this work, an adaptive-coefficient PSO strategy is employed to simultaneously optimize the three FOPI parameters, Kp, Ki, and λ. The inertia weight, cognitive coefficient, and social coefficient are varied during the optimization process to provide a progressive transition from exploration toward exploitation of promising regions of the search space.

The optimization criterion adopted in this work is centered on the Integral of Time-weighted Absolute Error (ITAE) [27-29], with additional terms incorporated to account for Integral Absolute Error (IAE), overshoot, settling time, control effort, and control-signal variation. Thus, the optimization does not rely solely on the tracking error but considers several aspects of the dynamic response. This ITAE-centered composite objective function is used to determine the FOPI parameters that provide an appropriate compromise between rapid error elimination, accurate reference tracking, limited overshoot, short settling time, and reasonable control action.

Based on these considerations, this paper proposes an APSO-optimized FOPI controller for DC-link voltage regulation of a single-phase AC–DC boost PFC converter. The proposed approach simultaneously optimizes Kp, Ki, and λ, while the Oustaloup approximation is employed to realize the fractional-order integrator in a form suitable for digital implementation. The performance of the optimized FOPI controller is evaluated against that of a conventional PI controller under both steady-state and dynamic operating conditions. The dynamic evaluation includes DC-link voltage reference transients and load-resistance variations, while the steady-state evaluation considers the input voltage and current waveforms, power factor, and input-current harmonic distortion.

The proposed control strategy is first investigated through MATLAB/Simulink simulations and is subsequently implemented in real time using a dSPACE 1104 control system. This simulation-to-experimental approach allows the dynamic and steady-state characteristics of the optimized FOPI controller to be evaluated under practical operating conditions. The experimental results are compared with the corresponding simulation results and with those obtained using the conventional PI controller.

The main contributions of this work are summarized as follows:

- Design of an FOPI voltage controller with the fractional integration order λ as an additional tuning parameter for DC-link voltage regulation.
- APSO-based optimization of Kp, Ki, and λ using an ITAE-centered composite objective function that considers tracking error, overshoot, settling time, control effort, and control-signal variation.
- Digital realization of the fractional-order integrator using the Oustaloup approximation followed by Tustin discretization for real-time implementation.
- Comprehensive comparison of the conventional PI and APSO-optimized FOPI controllers under steady-state and dynamic operating conditions, including DC-link voltage reference transients and load-resistance variations.
- Experimental validation using a dSPACE 1104 real-time control system, enabling comparison between simulation and experimental results and between the conventional PI and optimized FOPI controllers.

Overall, this study investigates the effectiveness of an APSO-optimized FOPI controller for improving the dynamic regulation of a single-phase boost PFC converter while maintaining satisfactory steady-state input-current quality and power-factor performance.

The remainder of this paper is organized as follows. Section 2 presents the mathematical modeling of the single-phase AC–DC boost PFC system. Section 3 describes the design of the FOPI controller and the Oustaloup approximation used for its realization. Section 4 presents the APSO optimization framework employed to determine the FOPI controller parameters. Section 5 presents and discusses the simulation results, including steady-state and dynamic performance under DC-link voltage reference and load-resistance variations. Section 6 presents and discusses the experimental results obtained using the dSPACE 1104 real-time control system and compares the performance of the conventional PI and optimized FOPI controllers. Finally, Section 7 concludes the paper.

2. The Plant Model and Controller Design

2.1. PFC Converter Model

The single-phase AC–DC boost PFC converter consists of a diode-bridge rectifier followed by a DC–DC boost converter, as shown in figure 1. The boost converter comprises an inductor L, a power switch (IGBT), a fast-recovery diode D, and an output capacitor C. A resistance R represents the load. The diode bridge converts the AC input voltage into a full-wave rectified voltage, while the boost stage regulates the DC-link voltage and shapes the input current to achieve power-factor correction[1-3] [6-9] [30-31].

The input voltage and current are assumed to be sinusoidal under ideal power-factor-correction conditions and can be expressed as:

$$v_s(t) = V_{max} sin(\omega t), \quad (2)$$

$$i_s(t) = I_{max}\, sin(\omega t) \quad (3)$$

Where $V_{max}$and I_{max} are the peak values of the source voltage and current, respectively, and ω is the angular frequency of the AC source.

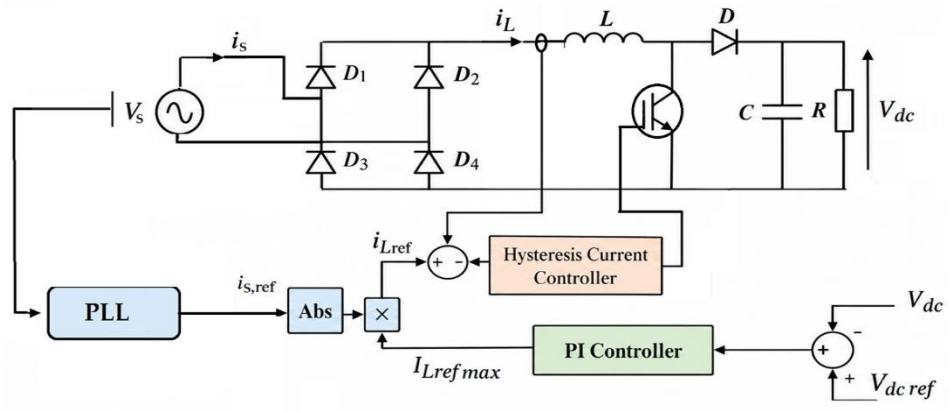

Figure 1. Single-phase AC-DC boost PFC converter topology

2.2. Dual-Loop Control Structure

The closed-loop control architecture of the PFC converter is shown in figure 2. The control system consists of a slow outer voltage loop and a fast inner current loop. The outer loop regulates the DC-link voltage, whereas the inner loop shapes the input current according to the reference generated by the voltage controller.

The measured DC-link voltage Vdc is compared with its reference value $V_{\mathrm{DC,ref}}$, producing the voltage error

$$e_v = V_{\mathrm{DC,ref}} - V_{\mathrm{DC}} \ldots\ldots\ldots (4)$$

For the conventional configuration, a PI controller processes the voltage error. For the proposed configuration, the same voltage-loop structure is equipped with the APSO-optimized FOPI controller. Thus, the two controllers are evaluated within the same PFC control architecture.

The instantaneous inductor-current reference is given by:

$$I_{l,\mathrm{ref}}\,(t) = I_{l,\mathrm{refmax}} * | \, sin(\omega t) \, | \cdots \ldots . (5)$$

The inner current loop employs a hysteresis-band controller to force the inductor current I_l to track $I_{l,\mathrm{ref}}$. The switching action of the IGBT is therefore determined by the instantaneous current tracking error. This control arrangement provides input-current shaping while maintaining the DC-link voltage around its reference value.

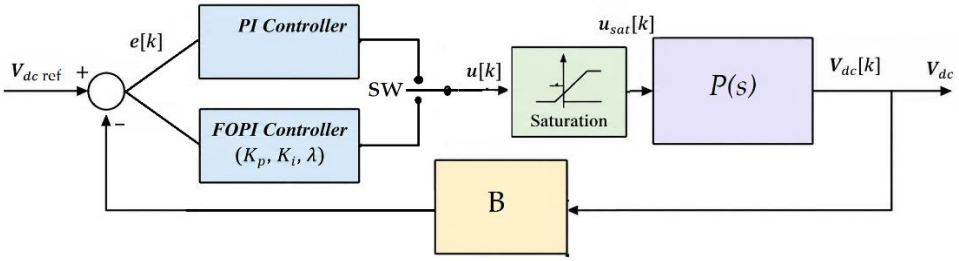

Figure 2. Closed-loop control architecture of the single-phase boost PFC converter.

Assuming ideal converter components and perfect current tracking ($I_l \approx I_{l,\mathrm{ref}}$), the power balance between the AC input and DC output can be expressed as:

$$\frac{V_{max}.I_{max}}{2} \cong V_{DC}(C.\frac{dV_{DC}}{dt} + \frac{V_{DC}}{R}) \quad (6)$$

with:

(6) can be rewritten as:

$$\frac{V_{DC}^2}{R} + \frac{C}{2}.\frac{dV_{DC}^2}{dt} = \frac{V_{max}I_{max}}{2} \quad (7)$$

Where Vmax Magnitude of the source voltage, Imax: Magnitude of source current, $\overline{V_{DC}}$ is the DC bus voltage at the operating point, and $(\overline{I})_{\max}$is the corresponding current amplitude.
with:

$$\begin{cases} V_{DC} = \bar{V}_{DC} + \tilde{V}_{DC} \\ I_{max} = \bar{I}_{max} + \tilde{I}_{max} \end{cases} \quad (8)$$

(7) is of a non-linear nature.
The linearization around the operating point gives the transfer function of the system:

$$\frac{\tilde{V}_{DC}}{\tilde{I}_{max}} = \frac{V_{max}}{4\bar{V}_{DC}}.\frac{R}{1+\frac{RC}{2}S} \quad (9)$$

The parameters of PI controller are calculated by dominant-pole compensation method as:

$$\begin{cases} K_p = \frac{RC}{2}Ki \\ K_i = \frac{1}{T_i} = \frac{8\pi f_c \bar{V}_{DC}}{BRV_{max}} \end{cases} \quad (10)$$

with:
Kp: Gain of proportional action.
Ki: Gain of integral action.
B: Attenuation of the measured output voltage, B=0.001.
fc: The voltage closed-loop crossover frequency, fc =5 Hz.
The system parameters used in this work are summarized in Table 1.

Table 1. Power circuit parameters

Parameters	Value
AC Source voltage (RMS) Ve	80 V
AC Source frequency f	50 Hz
DC bus voltage Vdc	120 V
DC bus capacitance C	1100 µF
DC boost converter inductance L	20 mH
Load resistance R	150 Ω

The PI controller is given by :

$$C(s) = 73.308 + 888.57\frac{1}{s} \quad (11)$$

The plant transfer function for the voltage loop, derived from power balance considerations, is given by:

$$P(s) = \frac{35.355}{(1 + 0.0825s)} \qquad (12)$$

This control-oriented model is used for the APSO-based optimization of the FOPI controller parameters. The optimization therefore focuses on the dynamic regulation of the DC-link voltage while accounting for tracking error, overshoot, settling time, control effort, and control-signal variation. The optimized controller is subsequently implemented on the experimental PFC converter using the dSPACE 1104 real-time control platform.

3. Fractional-Order PI Controller Design

3.1 Fundamentals of Fractional Calculus

Fractional calculus extends the conventional concepts of differentiation and integration to non-integer orders, providing an additional degree of freedom for controller design. In a fractional-order proportional-integral (FOPI) controller, the conventional integer-order integrator is replaced by a fractional-order integrator $s^{-\lambda}$, where λ denotes the fractional integration order[10-12].

For the voltage loop of the PFC converter, the FOPI controller is defined as:

$$G_{\mathrm{FOPI}}(s) = Kp + \frac{Ki}{s^{\lambda}} \qquad (13)$$

where Kp is the proportional gain, Ki is the integral gain, and λ is the fractional integration order.

In this work, the fractional-order parameter is constrained to $0<\lambda<1$. In the limiting case $\lambda=1$, the fractional-order integral becomes the conventional first-order integral, and the FOPI controller reduces to the classical PI controller.

$$G_{\mathrm{PI}}(s) = Kp + \frac{Ki}{s} \qquad (14)$$

Thus, compared with the conventional PI controller, the FOPI controller introduces λ as an additional tuning parameter, providing greater flexibility in shaping the dynamic response of the DC-link voltage control loop.

Because the ideal fractional-order operator $s^{-\lambda}$ cannot generally be implemented directly in a finite-dimensional digital controller, an appropriate approximation is required. Several methods have been investigated for the numerical realization of fractional-order operators, including the Grünwald–Letnikov formulation, continued-fraction expansion, and frequency-domain rational approximation techniques [10-13].

In this work, the Oustaloup recursive approximation is employed to obtain a finite-order rational approximation of the fractional integrator $s^{-\lambda}$ over a predefined frequency range.

The Oustaloup approximation distributes a set of poles and zeros over the selected frequency interval to reproduce the frequency-domain characteristics of the fractional-order operator. The resulting continuous-time rational approximation is subsequently discretized using the Tustin (bilinear) transformation to obtain the discrete-time representation required for digital implementation.

The open-loop transfer function of the DC-link voltage control loop can be expressed as:

$$G_{OL}(s) = C_{FOPI}(s)P(s), \qquad (15)$$

where P(s) represents the DC-link voltage plant given in Section 2.

Substituting the FOPI controller from (13) into (15) gives

$$G_{OL}(s) = \left(Kp + \frac{Ki}{s^{\lambda}}\right)P(s), \ldots\ldots\ldots (16)$$

The closed-loop transfer function is therefore

$$G_{CL}(s) = \frac{C_{\mathrm{FOPI}}(s)\mathrm{P(s)}}{\left(1 + B\ C_{\mathrm{FOPI}}(s)\ \mathrm{P(s)}\right)}, \ldots\ldots (17)$$

The FOPI controller contains three parameters, Kp, Ki, and λ, which are coupled through the closed-loop response. Their simultaneous selection affects the tracking error, overshoot, settling time, control effort, and control-signal variation. Therefore, rather than relying solely on manual tuning, the three parameters are optimized using the adaptive-coefficient PSO procedure described in Section 4.

3.2 Oustaloup Recursive Approximation

The Oustaloup approximation is a frequency-domain method used to approximate a fractional-order operator by an integer-order rational transfer function [14-16]. The method is based on the recursive distribution of poles and zeros over a predefined frequency interval. Because the frequency response of a fractional-order operator exhibits a constant slope in the logarithmic magnitude-frequency representation, an accurate approximation over the entire frequency spectrum is generally impractical. Therefore, the approximation is performed over a finite frequency band $[\omega_L, \omega_H]$.

Where ω_L and ω_H denote the lower and upper angular-frequency limits, respectively.

For a fractional operator $s^{-\lambda}$, the Oustaloup approximation of order N can be expressed in the general form:

$$G_O(s) = K_O \times \prod_{k=-N}^{N} \frac{(s + \omega_{z,k})}{(s + \omega_{p,k})} \dots\dots (18)$$

where $G_O(s)$ is the rational approximation of the fractional operator, K_O is the approximation gain, $\omega_{z,k}$ and $\omega_{p,k}$ are the zeros and poles, respectively, and N denotes the approximation order.

The poles and zeros are logarithmically distributed within the selected frequency range $[\omega_L, \omega_H]$according to the Oustaloup recursive formulation.

The zeros $\omega_{z,k}$, poles $\omega_{p,k}$, and gain K_O are defined as:

$$\omega_{z,k} = \omega_L \times \left(\frac{\omega_H}{\omega_L}\right)^{\frac{k+N+0.5(1+\lambda)}{2N+1}} \dots\dots\dots\dots\dots (19)$$

$$\omega_{p,k} = \omega_L \times \left(\frac{\omega_H}{\omega_L}\right)^{\frac{k+N+0.5(1-\lambda)}{2N+1}} \dots\dots\dots\dots\dots (20)$$

$$K_O = \omega_H^{-\lambda} \dots\dots\dots\dots\dots\dots\dots\dots\dots\dots\dots\dots\dots\dots\dots\dots (21)$$

where k=−N,−N+1,…,N−1,N.

For the FOPI controller, the fractional term in (13) is therefore replaced by the oustaloup approximation as:

$$C_{FOPI}(s) = K_p + K_i\, G_O(s) \dots\dots\dots\dots\dots\dots\dots\dots\dots (22)$$

This rational continuous-time controller is then discretized for real-time implementation.

3.3 Discretization Using the Tustin Transformation

Following the Oustaloup approximation, the continuous-time FOPI controller is converted into a discrete-time representation suitable for real-time implementation. The discretization is performed using the Tustin (bilinear) transformation [17], which maps the continuous-time s-domain into the discrete-time z-domain according to :

$$s = \left(\frac{2}{T_S}\right)\frac{(1 - z^{-1})}{(1 + z^{-1})} \dots\dots (23)$$

Where T_S is the sampling period.

Substituting (23) into the rational approximation $G_O(s)$ and, consequently, into (22), yields the discrete-time FOPI controller in the form:

$$C_{FOPI}(z) = \frac{B(z)}{A(z)}, \quad \dots\dots (24)$$

Equation (24) can be written as:

$$C_{FOPI}(z) = \frac{(b_0 + b_1 z^{-1} + b_2 z^{-2} + \ldots + b_M z^{-M})}{(a_0 + a_1 z^{-1} + a_2 z^{-2} + \ldots + a_M z^{-M})} \ldots\ldots (25)$$

where:

$$B(z) = b_0 + b_1 z^{-1} + b_2 z^{-2} + \ldots + b_M z^{-M} \ldots\ldots (26)$$

and

$$A(z) = a_0 + a_1 z^{-1} + a_2 z^{-2} + \ldots + a_M z^{-M} \ldots\ldots (27)$$

Here, M denotes the order of the resulting discrete-time controller.
After normalization, the leading denominator coefficient a_0 is set to unity, resulting in the standard form:

$$C_{FOPI}(z) = \frac{(b_0 + b_1 z^{-1} + b_2 z^{-2} + \ldots + b_M z^{-M})}{(1 + a_1 z^{-1} + a_2 z^{-2} + \ldots + a_M z^{-M})} \ldots\ldots (28)$$

The coefficients b_i and a_i are obtained from the discretized Oustaloup-based FOPI transfer function and constitute the discrete-time implementation coefficients of the FOPI controller. These coefficients are then used to implement the controller in the digital control system using the following difference equation:

$$u(k) = \sum_{i=0}^{M} b_i * e[k-i] - \sum_{i=1}^{M} a_i * u[k-i] \ldots\ldots (29)$$

Where e[k] is the sampled DC-link voltage error and u[k] is the controller output at sampling instant k.
This approach provides a systematic transition from the continuous fractional-order controller to its practical discrete-time realization, enabling implementation on digital control platforms such as dSPACE, and other programmable digital controllers.

4. Particle Swarm Optimization PSO-based optimal tuning

Particle Swarm Optimization (PSO), introduced by Kennedy and Eberhart, is a population-based optimization technique inspired by the collective behavior of social organisms such as bird flocks and fish schools [20–26]. The PSO search mechanism is based on the movement of particles toward both their individual best positions and the global best position found by the swarm. The velocity of each particle is updated according to:

$$v_{i(t+1)} = w * v_{i(t)} + c1 * r1 * (pbest_i - x_{i(t)}) + c2 * r2 * (gbest - x_{i(t)}) \ldots\ldots\ldots (30)$$

where $v_{i(t)}$ is the particle velocity, $pbest_i$ is the personal-best position, $gbest$ is the global-best position, w is the inertia weight, $c1$ is the cognitive coefficient, $c2$ is the social coefficient, and $r1$ and $r2$ are random numbers uniformly distributed between 0 and 1. The particle position is subsequently updated according to

$$x_{i(t+1)} = x_{i(t)} + v_{i(t+1)} \ldots\ldots\ldots\ldots (31)$$

4.1. Adaptive Particle Swarm Optimization Based on the ITAE Criterion

The PSO algorithm initializes a swarm of N particles, where each particle represents a candidate solution vector in the search space. In the present study, an Adaptive Particle Swarm Optimization (APSO) algorithm is employed to optimize the parameters of the fractional-order proportional-integral (FOPI) controller. The optimization variables are the proportional gain Kp, the integral gain Ki, and the fractional-order parameter λ. Therefore, the position of the i-th particle is defined as:

$$X_i = [K_{p,i}, K_{i,i}, \lambda_i] \quad \ldots\ldots\ldots\ldots (32)$$

Each particle consequently represents a candidate FOPI controller whose transfer function is expressed as:

$$G_{\mathrm{FOPI}}(s) = K_p + K_i.\frac{1}{s^{\lambda}}, \ldots\ldots\ldots\ldots (33)$$

For each candidate set of controller parameters, the closed-loop response of the Boost-PFC system is evaluated. The plant considered in the optimization is:

$$P(s) = \frac{35.355}{(1 + 0.0825s)}, \ldots\ldots\ldots\ldots (34)$$

The closed-loop transfer function of the voltage-control system is given by:

$$T(s) = \frac{C(s)P(s)}{1 + \mathrm{B}\, C(s)P(s)}, \ldots\ldots\ldots\ldots (35)$$

Since the fractional-order term $s^{-\lambda}$ cannot be directly represented by a conventional finite-order transfer function, an Oustaloup recursive approximation is employed. In the MATLAB implementation, an approximation order of one is used over the frequency range from 0.01 to 5000 rad/s.

The performance of each candidate FOPI controller is evaluated using a composite objective function. The tracking error is defined as:

$$e(t) = r(t) - y(t)\,, \ldots\ldots\ldots\ldots (36)$$

Where $r(t)$ is the reference signal and $y(t)$ is the closed-loop output. A unit-step reference is used during the optimization; therefore,

$$r(t) = 1 \quad and \quad e(t) = 1 - y(t).\,, \ldots\ldots\ldots\ldots (37)$$

The Integral of Time-weighted Absolute Error (ITAE) is calculated as:

$$J_{ITAE} = \int_0^T t * |e(t)|\, dt \ldots\ldots\ldots (38)$$

where T represents the evaluation time interval. In the numerical implementation, the integral is approximated using the sampled response:

$$J_{ITAE} = \sum_{\mathrm{k=0}}^{\mathrm{N}} t_k \ |e(t_k)| * \ \Delta t \ldots\ldots\ldots\ldots\ldots (39)$$

where t_k is the k-th sampling instant, Δt is the sampling interval, and N is the number of samples. The time-weighting factor t gives greater importance to errors that persist for longer periods. Consequently, minimizing the ITAE criterion encourages rapid elimination of the tracking error and improves the settling characteristics of the closed-loop response.

To prevent the optimizer from selecting an excessively aggressive controller that achieves a fast response at the expense of output-voltage overshoot, an additional overshoot penalty is incorporated into the objective function.

In addition to ITAE, the Integral of Absolute Error (IAE) is included in the objective function:

$$J_{IAE} = \int_0^T |e(t)|\, dt \ldots\ldots\ldots (40)$$

The inclusion of IAE complements the ITAE term by penalizing the overall accumulated tracking error.
For a unit-step reference:

$$r(t) = 1 , \ldots\ldots\ldots\ldots (41)$$

To limit excessive transient overshoot, an overshoot penalty is also introduced. For the unit-step response, the normalized overshoot is calculated as:

$$M_p = \max(0, \frac{\max(\mathrm{y}) - \mathrm{r}}{r}) , \ldots\ldots\ldots\ldots (42)$$

Thus, $Mp = 0$ when the output does not exceed the reference value. The corresponding overshoot penalty is defined as :

$$J_{OS} = \alpha M_p^2 , \ldots\ldots\ldots\ldots (43)$$

The settling time is also incorporated into the optimization criterion. The settling time ts is determined using a 2% settling band around the reference value. This term encourages the optimization algorithm to obtain a faster transient response.
Furthermore, the controller effort is considered through the RMS value of the control signal,

$$U_{RMS} = \sqrt{\frac{1}{T}\int_0^T u^2 dt} , \ldots\ldots\ldots\ldots (44)$$

Together with the accumulated variation of the control signal. These terms discourage unnecessarily large and rapidly varying control actions.
Consequently, the complete objective function implemented in the optimization is

$$J = ITAE + 0.01\, IAE + 20M_P^2 + 0.1 * ts + 10^{-4} * U_{RMS}^2 + 10^{-5} * V_u, \ldots\ldots\ldots\ldots (45)$$

Where V_u represents the accumulated control-signal variation.
This formulation therefore evaluates the FOPI controller according to tracking accuracy, transient overshoot, settling time, control effort, and control-signal variation, rather than relying solely on the ITAE criterion. Unstable or non-finite closed-loop responses are rejected by assigning a large penalty value to the corresponding candidate solution.

4.2 PSO Configuration and Adaptive Coefficients

One particle is initialized using the classical PI gains with (λ =1.0), while the remaining particles are randomly initialized within the search bounds. The APSO coefficients are adaptively adjusted according to the normalized iteration factor k, with w and c_1 decreasing from 0.9 to 0.3 and 2.5 to 0.5, respectively, while the c_2 increases from 0.5 to 2.5. This adaptation promotes exploration during the initial iterations and progressively enhances exploitation and convergence toward the global-best solution.

The optimization is performed using 30 particles over a maximum of 40 iterations. The FOPI parameters are constrained by $0.01 \leq Kp \leq 100$ $0.01 \leq Ki \leq 300$ and $0.10 \leq \lambda \leq 0.9$

At each iteration, the fitness of each particle is evaluated, and the personal-best and global-best positions are updated. The process continues until the maximum number of iterations is reached, yielding the optimal parameter vector:

After evaluating the fitness of all particles, the personal-best and global-best positions are updated. This process is repeated until the maximum number of iterations is reached. Finally, the global-best particle provides the optimized FOPI parameters:

$$X^* = \left[K_p^*, K_i^*, \lambda^*\right], \ldots\ldots\ldots\ldots\ldots\ldots (46)$$

where K_p^* is the optimal proportional gain, K_i^* is the optimal integral gain, and $\lambda^*$is the optimal fractional-order parameter of the FOPI controller.

The resulting parameters correspond to the FOPI controller that minimizes the defined composite objective function, which aims to improve tracking performance, reduce steady-state error and settling time, limit output-voltage overshoot, and maintain reasonable control effort.

5. SIMULATION RESULTS

The complete system (figure 1), including the power circuit and the FOPI-based control algorithm, is simulated under MATLAB/Simulink R2018a using the Control System Toolbox.

5.1 APSO Optimization Results

APSO-based FOPI optimization using the ITAE-centered composite objective function is presented in Figure 3, showing the convergence of the objective function and the resulting transient tracking performance.

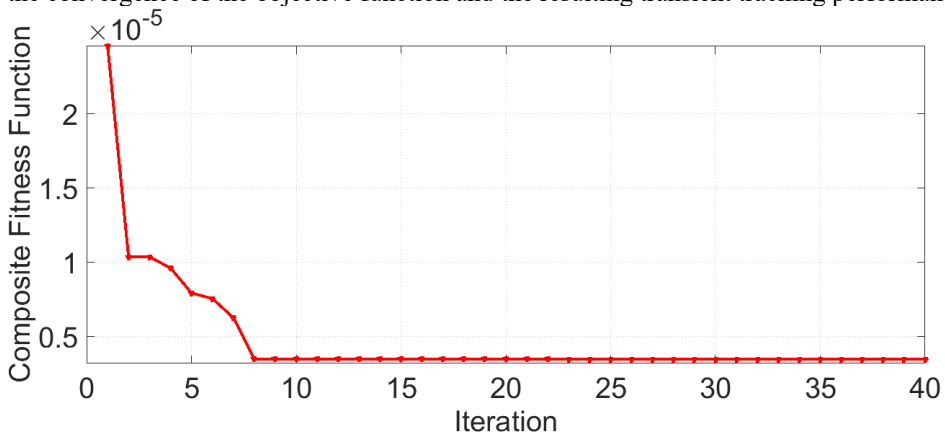

Figure 3. Convergence of the APSO-based FOPI optimization using the ITAE-centered composite objective function.

The obtained FOPI gain using APSO are summarized in table 2.

Table 2. Optimized FOPI controller parameters obtained using the APSO algorithm.

Parameters	Value
Kp	50.0
Ki	270.864679
λ	0.85
Composite objective J	0.000003

The fractional integrator was approximated using the Oustaloup recursive filter method, yielding the following discrete (Tustin method) transfer function coefficients:

b = [50.197827446679,-150.542125981913,150.490773327275, -50.146474792023];
a = [1.000000000000, -2.999114668851, 2.998229347458, -0.999114678607];

The Oustaloup parameters used for the discretization are summarized in Table 3.

Table 3. Oustaloup parameters.

Parameter	Symbol	Value
Lower frequency bound	ω_L	0.01 rad/s
Upper frequency bound	ω_H	5000.0 rad/s
Approximation order	N	1
SAMPLE TIME	T_S	30 µs

To validate the performance of the AC-DC boost PFC converter, a series of simulation tests are conducted using MATLAB/Simulink under various operating conditions for both the classic PI and FOPI controllers.

5.2 Classical PI Controller Simulation Results

5.2.1 Steady-State Performance

The steady-state source voltage and current waveforms obtained with the classical PI controller are illustrated in Figure 4. The converter draws a near-sinusoidal source current that is synchronized in phase with the source voltage, confirming near-unity power factor operation (0.9995). Under these conditions, the PI controller achieves an input current Total Harmonic Distortion (THD) of 3.02% with a fundamental component of 1.797 A (Figure 4(c)), satisfying standard power quality requirements.

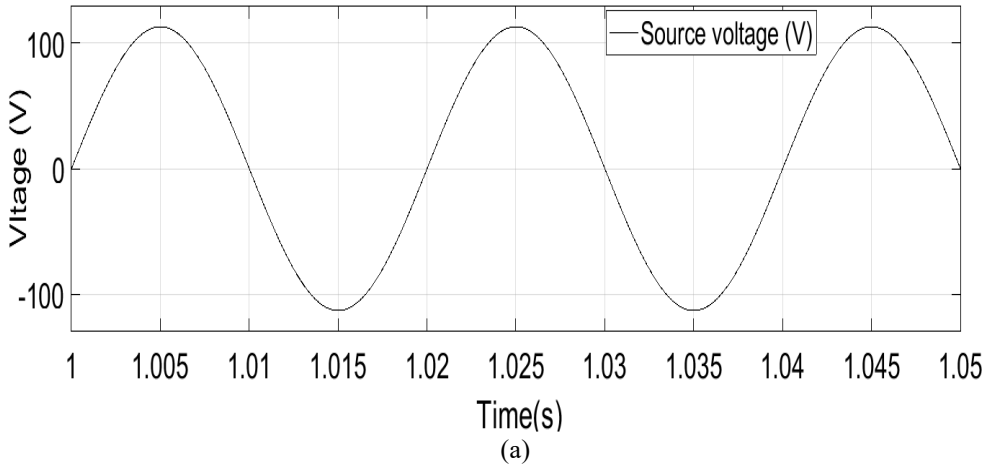

(a)

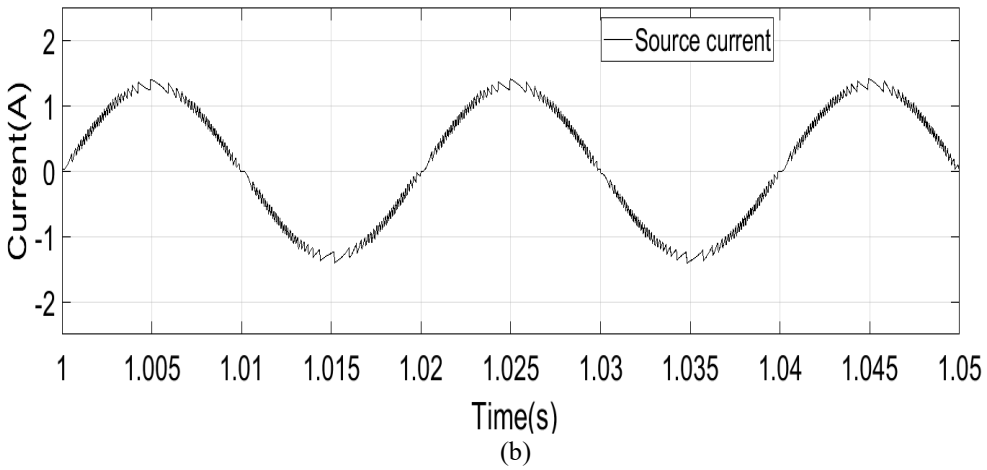

(b)

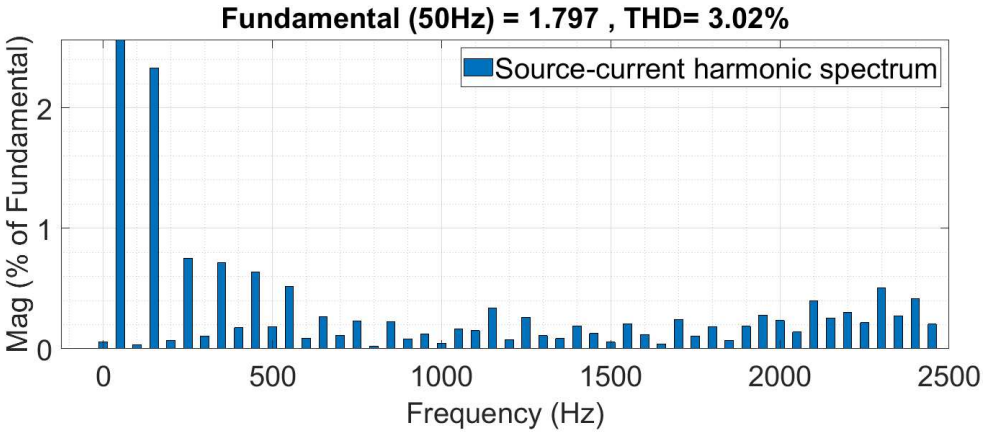

(c)

Figure. 4 Steady-state waveforms using the PI controller: (a) source voltage, (b) source current, and (c) source-current harmonic spectrum.

5.2.2 Dynamic Performance

To evaluate the dynamic performance of the classical PI-controlled PFC converter, two transient tests are conducted: a step change in the DC bus voltage reference and a step change in the resistive load.

5.2.2.1 DC-Bus Voltage Reference Step

Figure 5, presents the simulation results of the classical PI-controlled PFC converter under DC bus voltage reference steps from 120 V to 140 V and back to 120 V. As shown in Figure. 5(a), the DC bus voltage smoothly tracks the reference and settles within approximately 200 ms for both transitions, exhibiting negligible overshoot. Correspondingly, Figure. 5(b) demonstrates that the source current amplitude increases and decreases to match the varying power demand, with only minor transient spikes at the step instants.

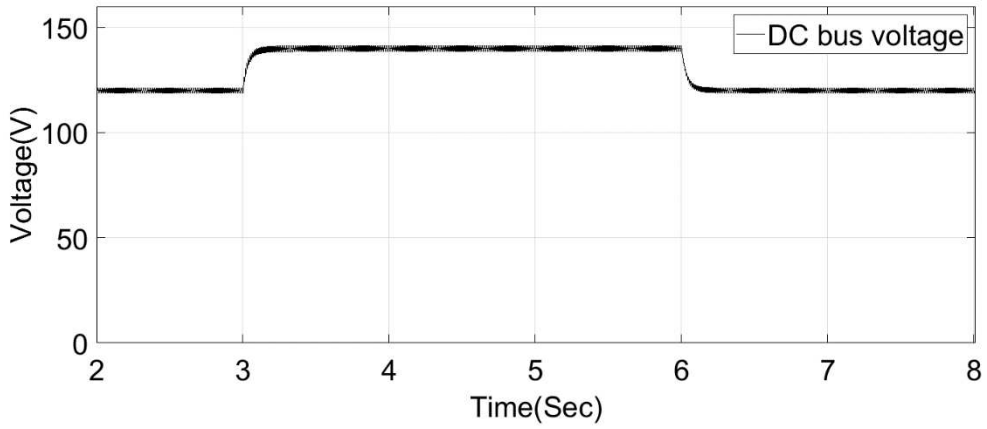

(a)

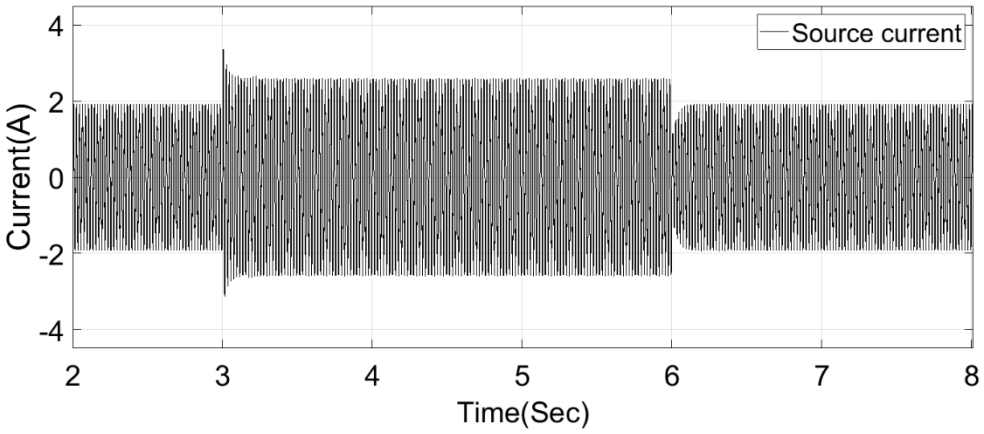

(b)

Figure 5. Simulation results using PI controller for the step change dc bus voltage (Increasing from 120 V to 140 V and decreasing from 140 V to 120 V): (a) DC bus voltage, (b) Source current

5.2.2.2 A resistive load step change

The simulated transient response of the classical PI-controlled PFC converter under a resistive load step change from 150 Ω to 100 Ω and back to 150 Ω is presented in Figure 6. When the load decreases to 100 Ω at t = 3 s, the DC bus voltage exhibits an 8 V undershoot and recovers to its nominal value within approximately 300 ms, while the source current amplitude increases to meet the higher power demand. When the load is restored to 150 Ω at t = 6 s, the DC bus voltage shows an 8 V overshoot and again settles within approximately 300 ms, accompanied by a reduction in source current amplitude.

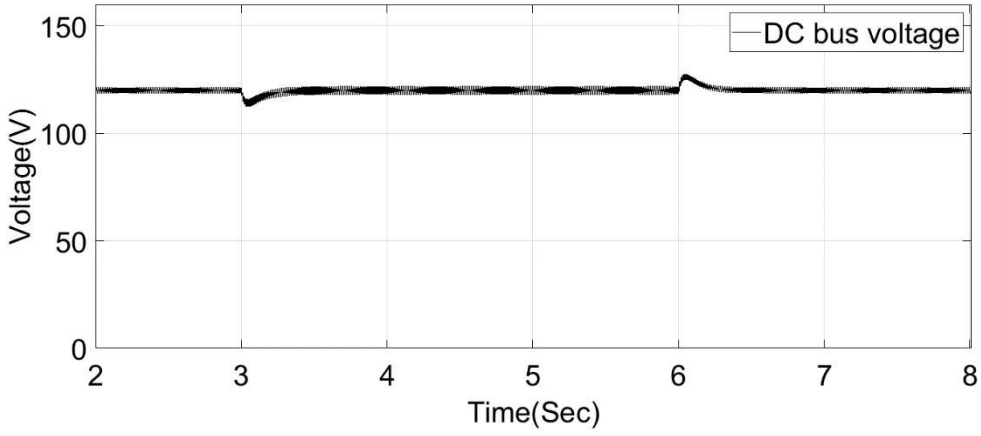

(a)

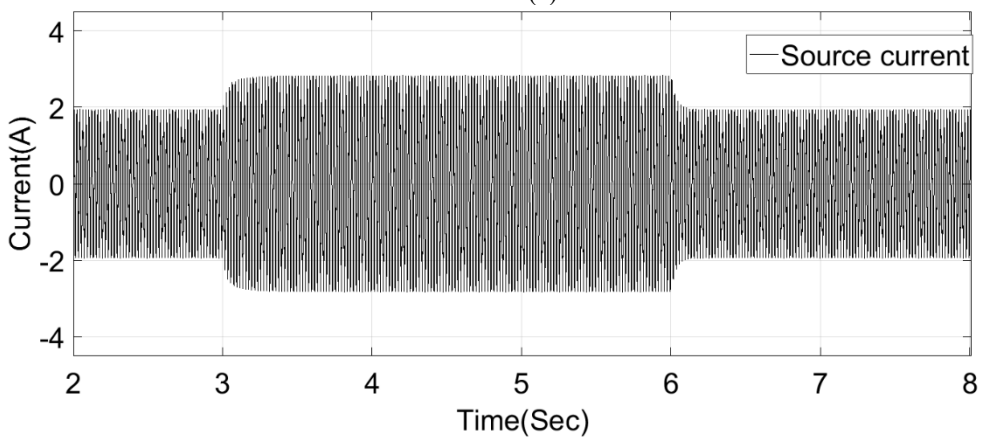

(b)

Figure 6. Simulation results using PI controller for the step change of resistive load (decreasing from 150 Ω to 100 Ω and increasing from 100 Ω to 150 Ω): (a) DC bus voltage, (b) Source current

5.3 FOPI Controller Simulation Results

5.3.1 Steady-State Performance

The steady-state waveforms and harmonic spectrum of the source voltage and current using the FOPI controller are presented in Figure 7. The source current is sinusoidal and in phase with the source voltage, indicating near-unity power factor operation, as shown in Figures 7((a) and (b)). The harmonic spectrum in Figure. 7(c) shows a fundamental current amplitude of 1.801A and a current THD of 4.39%, which complies with the IEEE 519 harmonic standard (<5%).

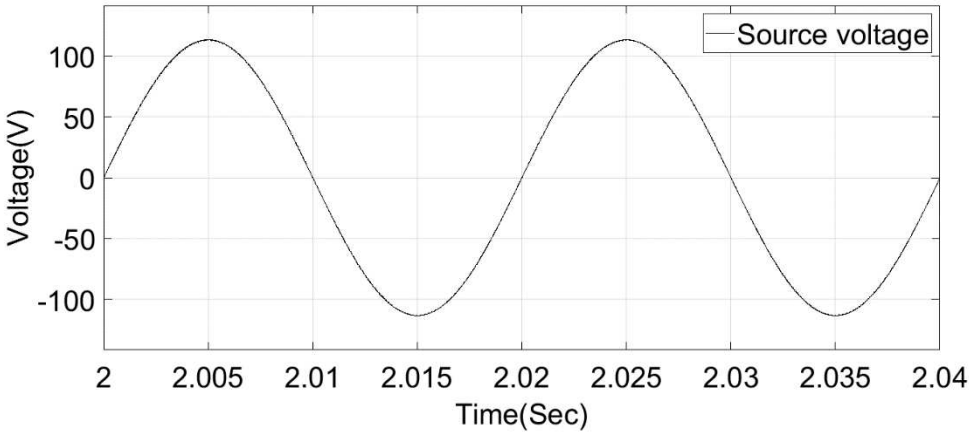

(a)

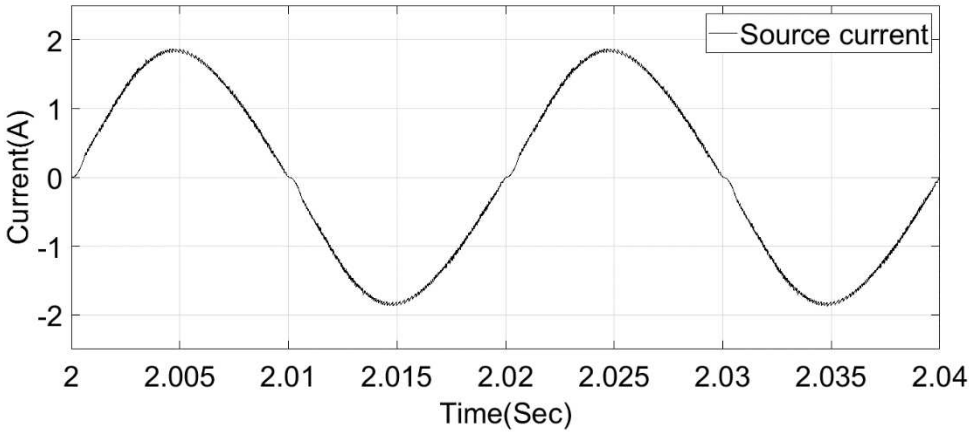

(b)

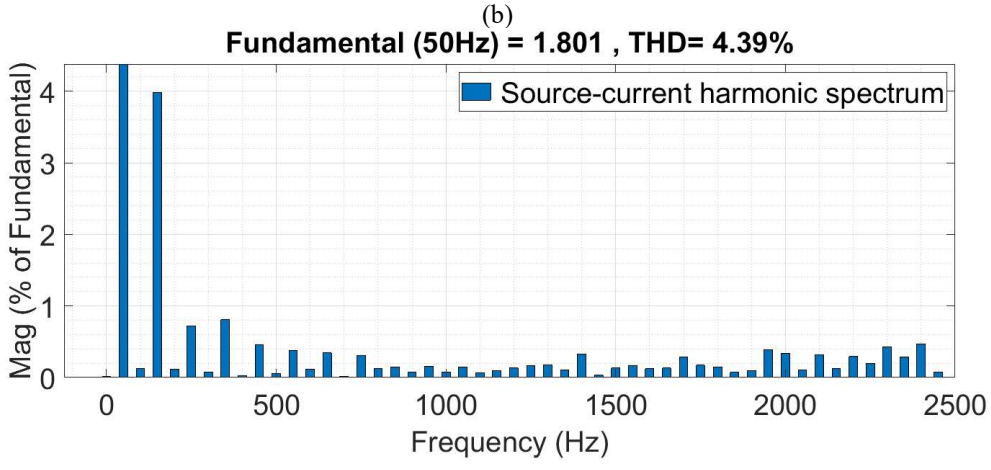

(c)

Figure 7. Steady-state waveforms using the FOPI controller: (a) source voltage, (b) source current, and (c) source-current harmonic spectrum.

5.3.2 Dynamic Performance

The dynamic performance of the FOPI-controlled PFC converter is assessed through two transient tests: a DC bus voltage reference step and a resistive load step.

5.3.2.1 A step change in dc bus voltage

Figure 8 presents the simulation results of the FOPI-controlled PFC converter under DC bus voltage reference steps from 120 V to 140 V and back to 120 V. As shown in Figure. 8(a), the DC bus voltage tracks the new reference and settles within approximately 50 ms for both transitions, exhibiting negligible overshoot. Correspondingly, Figure. 8(b) shows that the source current amplitude increases and decreases to match the varying power demand, with only minor transient spikes at the step instants.

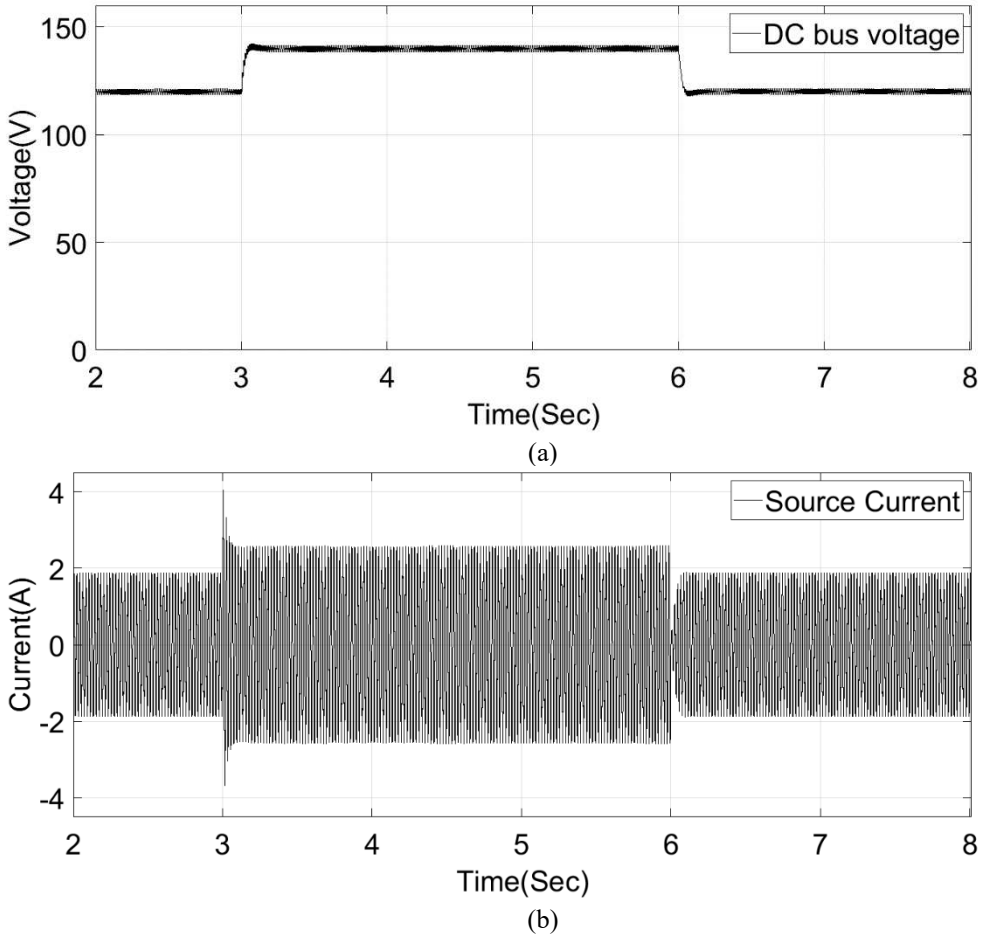

Figure 8. Simulation results using FOPI controller for the step change dc bus voltage (Increasing from 120 V to 140 V and decreasing from 140 V to 120 V): (a) DC bus voltage, (b) Source current.

5.3.2.2 A resistive load step change

The dynamic performance of the FOPI-controlled PFC converter under step variations in the load resistance are illustrated in Figure 9, decreasing from 150 Ω to 100 Ω and increasing back to 150 Ω. As shown in Figure. 9(a), the DC bus voltage remains tightly regulated at its nominal value with negligible transient deviation during both load transitions. Correspondingly, Figure. 9(b) shows that the source current amplitude increases at t = 3 s to meet the higher power demand and decreases at t = 6 s when the load is restored, with only minor transient spikes.

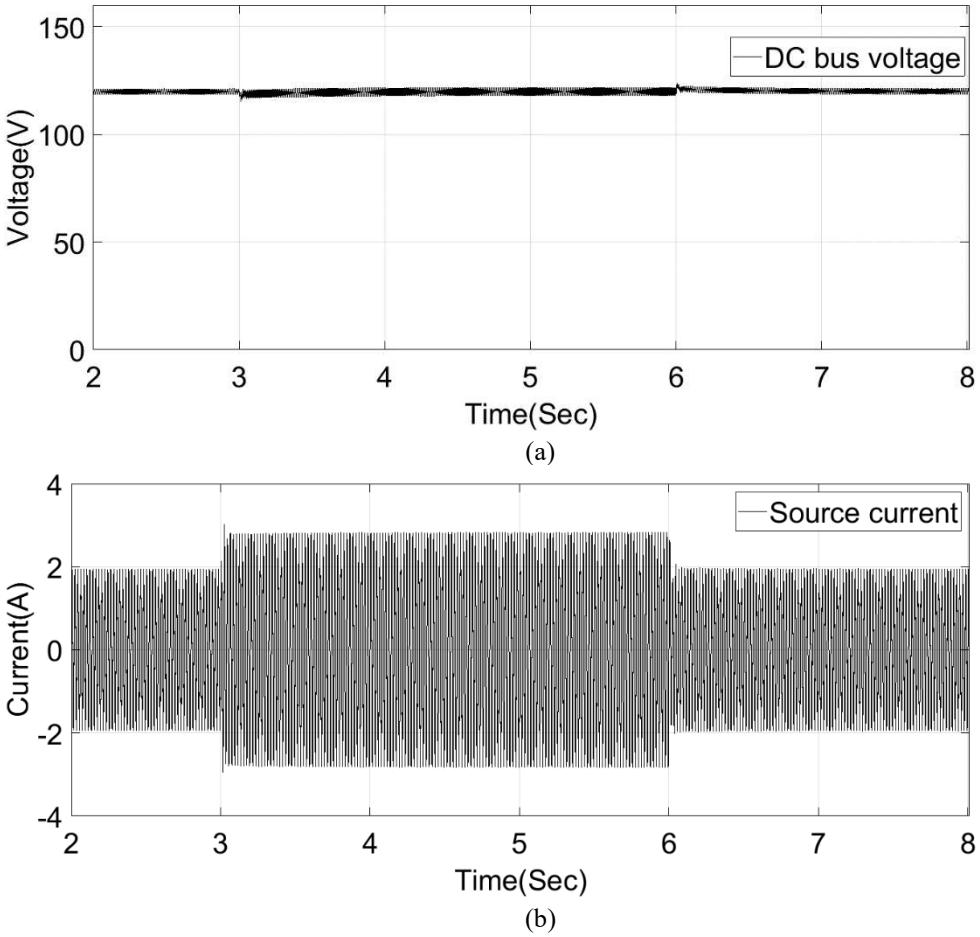

Figure 9. Simulation results to load resistance step changes decreasing from 150 Ω to 100Ω and increasing from 100 Ω to 150 Ω): (a) DC bus voltage and (b) source current.

5.4 Comparative Discussion of PI and FOPI

A comprehensive evaluation of the classical PI and optimized FOPI controllers for the Boost PFC converter are given in table 4.

Both controllers exhibit comparable steady-state performance. The current THD remains below the 5% IEEE 519 limit for both controllers (3.02% for PI and 4.39% for FOPI), with nearly identical fundamental current amplitudes (1.797 A and 1.801 A, respectively). Both achieve near-unity power factor (~0.999), confirming excellent steady-state power quality.

The FOPI controller demonstrates a significant improvement in transient response, achieving a settling time of approximately 50 ms compared to 200 ms for the classical PI controller. This represents a 75% reduction in settling time (4-time faster response). Both controllers exhibit negligible overshoot and comparable source current transient behavior with minor spikes. This indicates that the FOPI controller tracks reference changes much faster without compromising damping or inducing additional current stress.

The superiority of the FOPI controller is most evident under load disturbance conditions. The FOPI controller settles within approximately 50 ms, while the classical PI controller requires approximately 300 ms, representing an 83.3% reduction in settling time (6-time faster response). More importantly, the classical PI controller exhibits an 8 V undershoot/overshoot in the DC bus voltage, whereas the FOPI controller maintains the voltage with negligible deviation. This demonstrates the FOPI controller's superior disturbance rejection capability. Both controllers show comparable source current transient behavior with minor spikes during load transitions.

Table 4: Simulation Comparison between Classical PI and Optimized FOPI Controllers

Performance Metric		Classical PI Controller	Optimized FOPI Controller	Improvement
Kp		73.308	50.0000	/
Ki		888.577	270.8647	/
Lambda (λ)		1.0000	0.8500	/
Steady-State	Current THD (%)	3.02%	4.39%	Comparable (both < 5%)
	Fundamental Current (A)	1.797 A	1.801 A	Nearly identical
	Power Factor	0.9995	0.9990	Near-unity for both
DC Bus Voltage Step (120 V ↔ 140 V)	Settling Time (ms)	~200 ms	~50 ms	75% reduction (4 time faster)
	Overshoot/Undershoot	Negligible	Negligible	Comparable
	Source Current Transient	Minor spikes	Minor spikes	Comparable
Resistive Load Step (150 Ω ↔ 100 Ω)	Settling Time (ms)	~300 ms	~50 ms	83.3% reduction (6 time faster)
	DC Bus Undershoot/Overshoot	8 V	Negligible	Significant improvement
	Source Current Transient	Minor spikes	Minor spikes	Comparable

6. Experimental Results

The optimized FOPI controller, obtained using the control-oriented simulation model, was implemented on the experimental single-phase boost PFC converter using the dSPACE 1104 real-time control platform. The experimental setup is shown in figure.10, comprising the AC source, diode bridge rectifier, boost converter, spectrum analyzer, and dSPACE 1104 platform. This setup enables the practical evaluation of the proposed controller under the operating conditions of the physical converter. To evaluate the performance of the complete power factor correction (PFC) system, three operating conditions were investigated: operation without PFC, operation with the conventional PI-controlled PFC, and operation with the proposed APSO-optimized FOPI-controlled PFC.

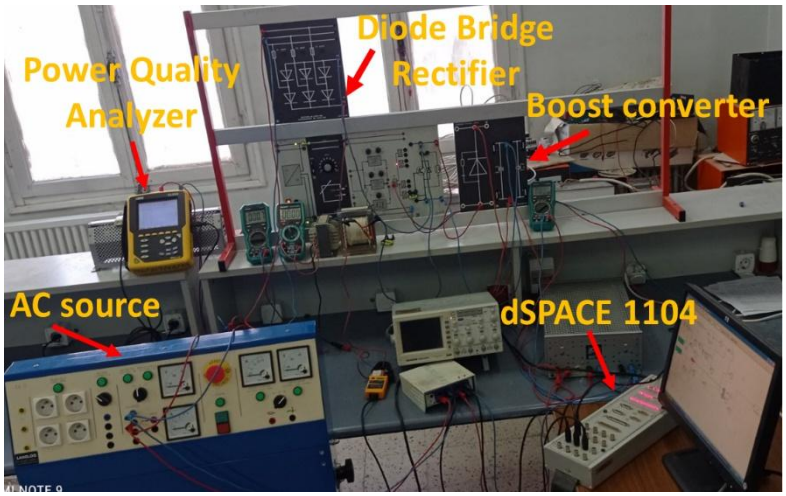

Figure 10. Experimental setup of the single-phase boost PFC converter,

6.1 Experimental Results Without PFC

Figure 11 presents the experimental results without PFC. The source current is highly distorted, exhibiting a current THD of 86.3%. The true power factor is only 0.743, despite a displacement power factor (DPF) of 0.992 and a fundamental phase shift of only 7°. This confirms that the low power factor is primarily caused by harmonic distortion rather than fundamental phase shift. Furthermore, the source current waveform is peaky and non-sinusoidal, which is characteristic of non-linear loads.

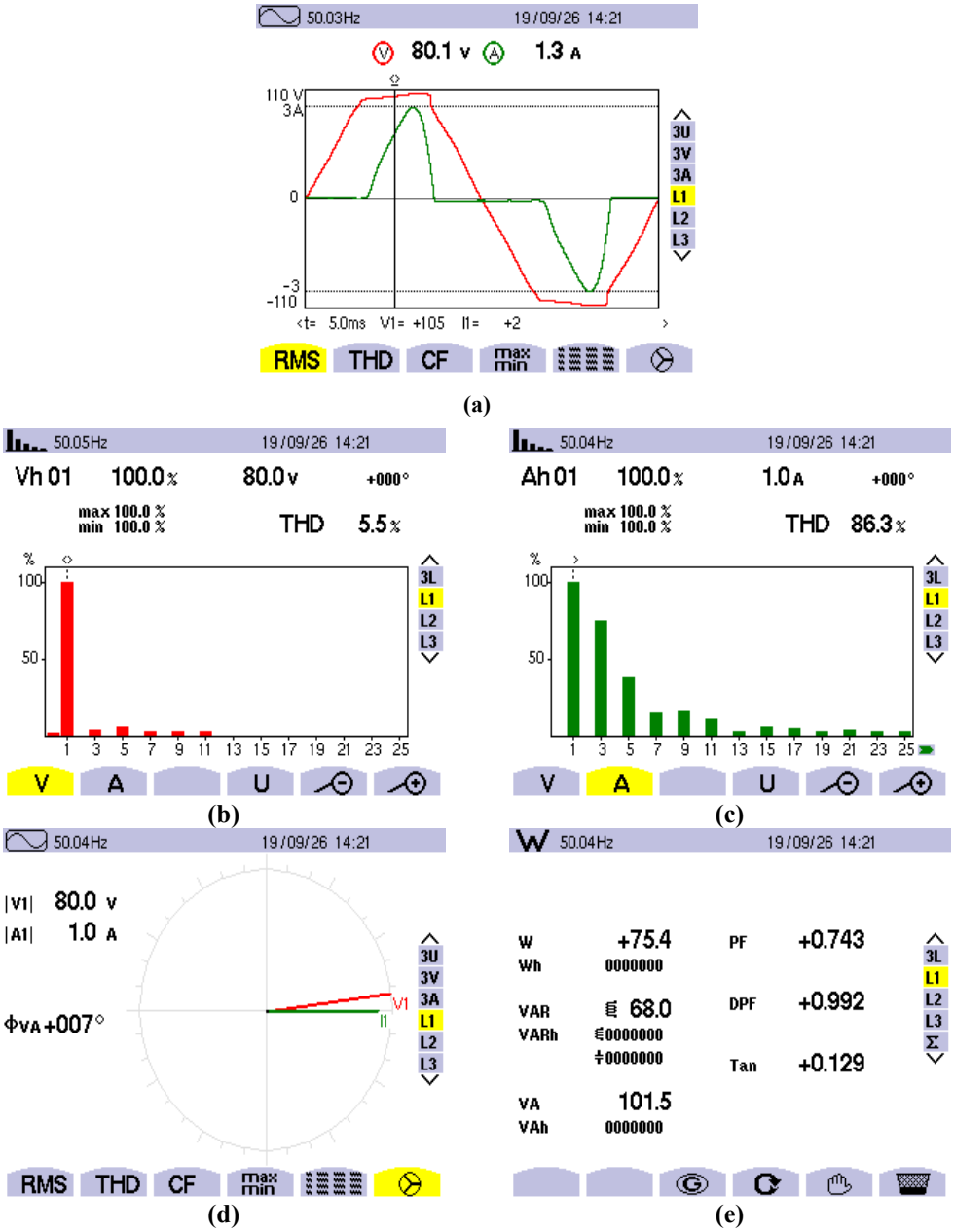

Figure 11. Experimental results under steady-state operation without power factor correction : (a) source voltage and current; (b) source-voltage harmonic spectrum; (c) source-current harmonic spectrum; (d) vector diagram; (e) experimental measurements.

6.2 Experimental Results with Classical PI

6.2.1 Steady-State Performance

The steady-state results employing a classical PI controller for power factor correction are presented in Figure 12. The controller effectively shapes the source current to be sinusoidal and in phase with the voltage (2° displacement), reducing the current THD to 3.4%. Consequently, the system achieves a near-unity power factor

of 0.998 (DPF = 0.999) with minimal reactive power (7.9 VAR). These results validate the classical PI controller's efficacy in mitigating harmonic distortion and achieving near-perfect power factor correction.

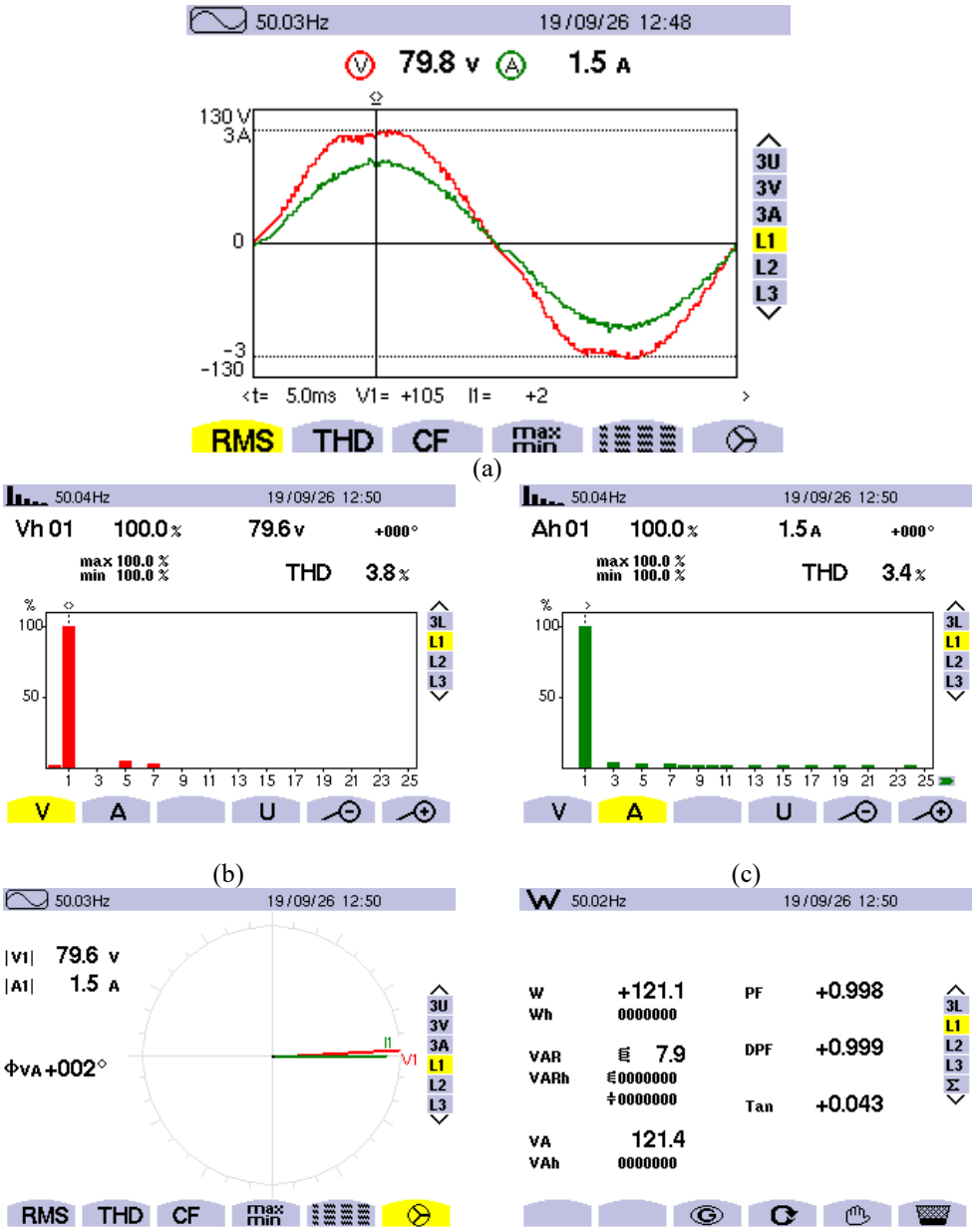

Figure 12. Experimental results under steady-state operation with power factor correction using a classical PI controller: (a) source voltage and current waveforms; (b) source-voltage harmonic spectrum; (c) source-current harmonic spectrum; (d) vector diagram; (e) experimental measurements.

The experimental steady-state waveforms of the classical PI-controlled PFC converter are presented in figure 13. As observed, the source voltage and source current exhibit sinusoidal waveforms, indicating that the input current is in phase with the source voltage. The DC-link voltage remains regulated around its reference value. These results confirm the steady-state operation of the conventional PI-controlled PFC converter and its capability to achieve input-current shaping with near-unity power-factor operation.

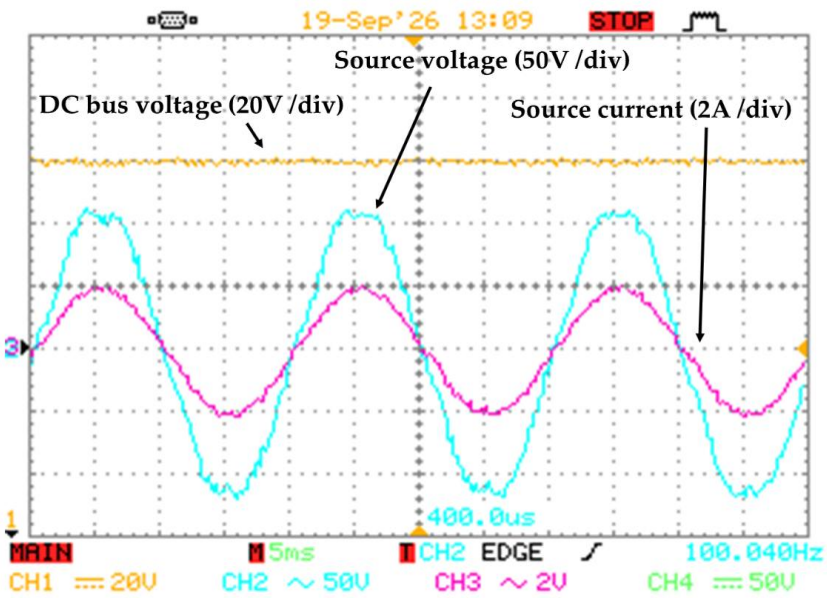

Figure 13. Experimental steady-state waveforms of the classical PI-controlled PFC converter.

6.2.2 Dynamic Performance

The dynamic performance of the classical PI-controlled PFC converter is assessed through two transient tests: a DC bus voltage reference step and a resistive load step.

6.2.2.1 A step change in dc bus voltage

Figure 14 show the experimental transient response of the classical PI-controlled PFC converter for successive DC-link voltage reference steps from 120 V to 140 V and from 140 V back to 120 V. In both cases, the DC-link voltage reaches the new reference level within approximately 200 ms, while the source-current amplitude changes accordingly during each transition.

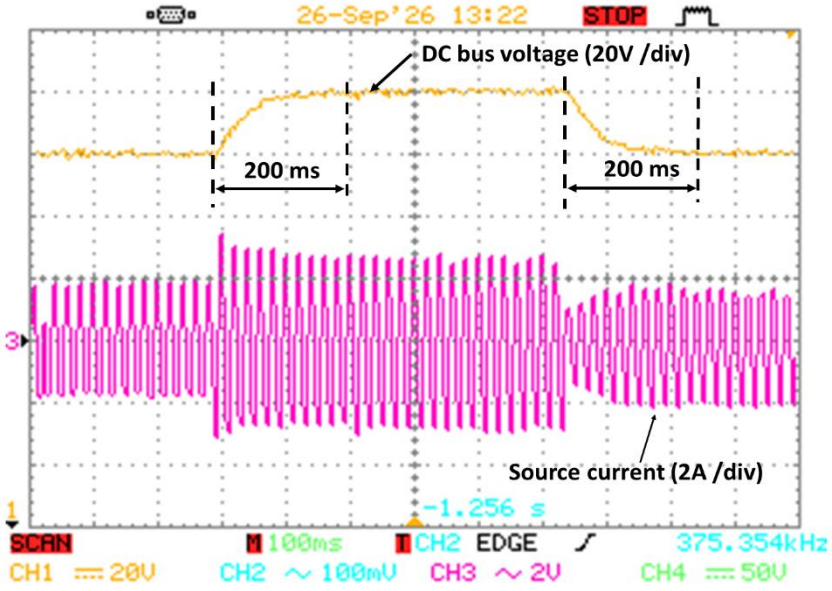

Figure 14. Experimental transient response of the classical PI-controlled PFC converter under successive DC-link voltage reference steps from 120 V to 140 V and back to 120 V.

6.2.2.2 A resistive load step change

Figure 15 presents the experimental load-transient response of the conventional PI-controlled PFC converter for a load resistance change from 150 Ω to 100 Ω and subsequently back to 150 Ω. When the load resistance is reduced to 100 Ω, the increased power demand produces an 8 V undershoot in the DC-link voltage, followed by recovery to its nominal value within approximately 300 ms. The corresponding increase in source-current amplitude reflects the higher input power required by the increased load. When the load resistance is restored to 150 Ω, the DC-link voltage exhibits an 8 V overshoot and returns to its steady-state value within approximately 300 ms, accompanied by a reduction in the source-current amplitude.

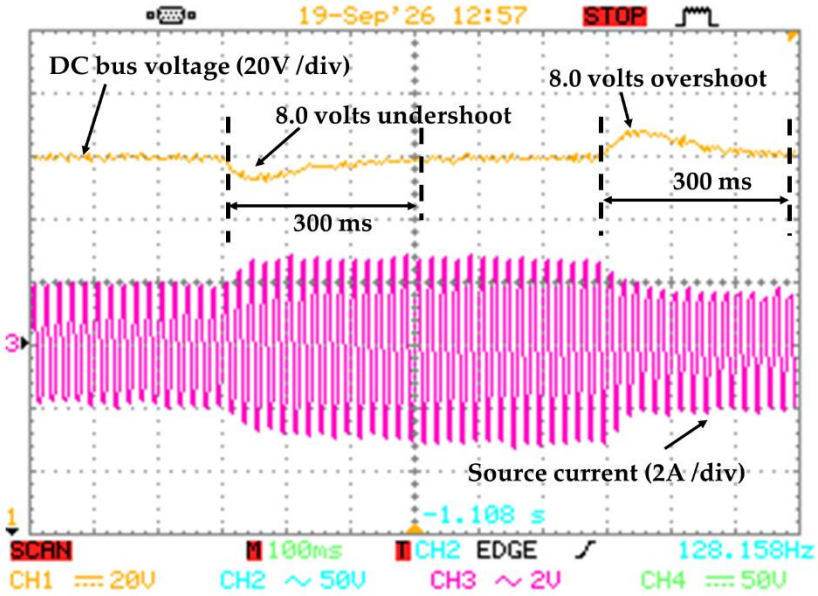

Figure 15. Experimental load-transient response of the classical PI-controlled PFC converter for load resistance changes from 150 Ω to 100 Ω and back to 150 Ω.

6.3 Experimental Results with FOPI controller

6.3.1 Steady-State Performance

Figure 16 presents the steady-state results employing a FOPI controller for power factor correction. The controller achieves a sinusoidal source current in phase with the voltage (3° displacement), reducing the current THD to 4.3% and voltage THD to 3.4%. Consequently, the system attains a near-unity power factor of 0.997 (DPF = 0.999) with minimal reactive power (8.7 VAR). These results validate the FOPI controller's efficacy in mitigating harmonic distortion and achieving near-perfect power factor correction.

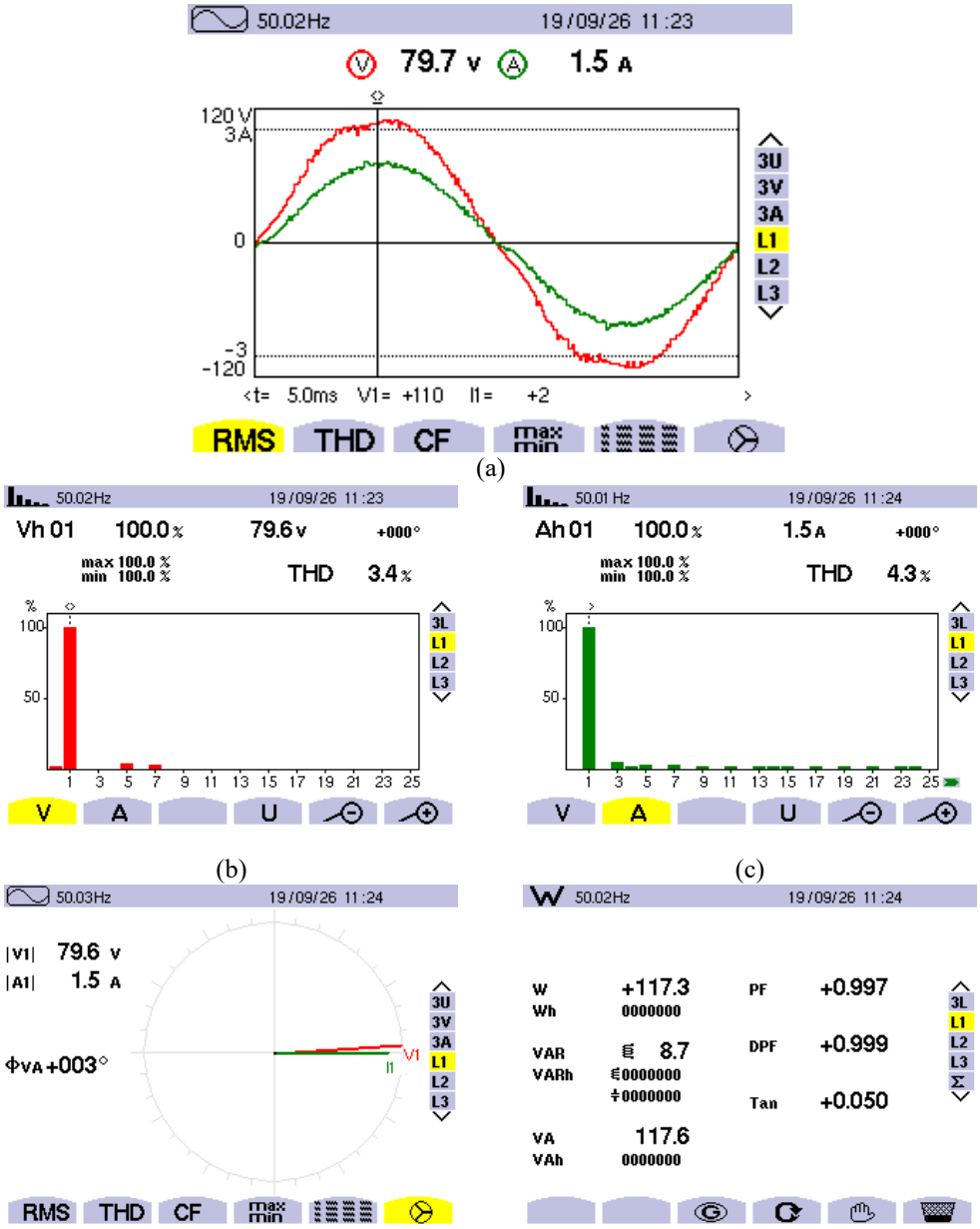

Figure 16. Experimental results under steady-state operation with power factor correction using a FOPI controller: (a) source voltage and current waveforms; (b) source-voltage harmonic spectrum; (c) source-current harmonic spectrum; (d) vector diagram; (e) experimental measurements.

Figure 17 shows the steady-state experimental waveforms of the PFC converter under FOPI control. The source voltage and source current exhibit a sinusoidal waveform with the current closely aligned in phase with the source voltage, indicating near-unity power-factor operation. The current waveform follows the polarity and zero crossings of the source voltage throughout the AC cycle, confirming that the FOPI-controlled converter effectively shapes the input current according to the grid voltage. Meanwhile, the DC-link voltage remains regulated at its reference value. These results demonstrate the satisfactory steady-state PFC performance and sinusoidal input-current shaping achieved by the implemented FOPI controller.

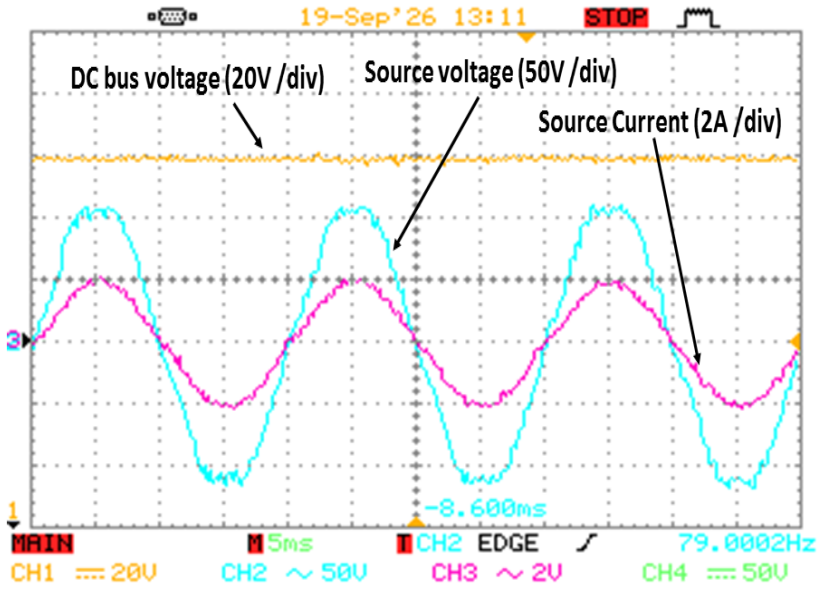

Figure 17. Experimental steady-state waveforms of the FOPI-controlled PFC converter : source voltage and source current in phase, with the regulated DC-link voltage

6.3.2 Dynamic Performance

The dynamic performance of the FOPI-controlled PFC converter is assessed through two transient tests: a DC bus voltage reference step and a resistive load step.

6.3.2.1 A step change in dc bus voltage

Figure 18 presents the experimental transient response of the FOPI-controlled PFC converter for successive DC-link voltage reference changes from 120 V to 140 V and then from 140 V back to 120 V. For the upward reference step, the DC-link voltage increases smoothly from 120 V to 140 V and reaches the new steady-state level within approximately 60 ms. The corresponding increase in source-current amplitude reflects the additional input power required during the voltage transition. When the reference is subsequently reduced from 140 V to 120 V, the DC-link voltage returns to its initial value within approximately 60 ms, accompanied by a reduction in source-current amplitude. The absence of significant voltage overshoot or undershoot and the similar transient durations for both reference changes indicate a well-damped and symmetric dynamic response of the experimentally implemented FOPI controller.

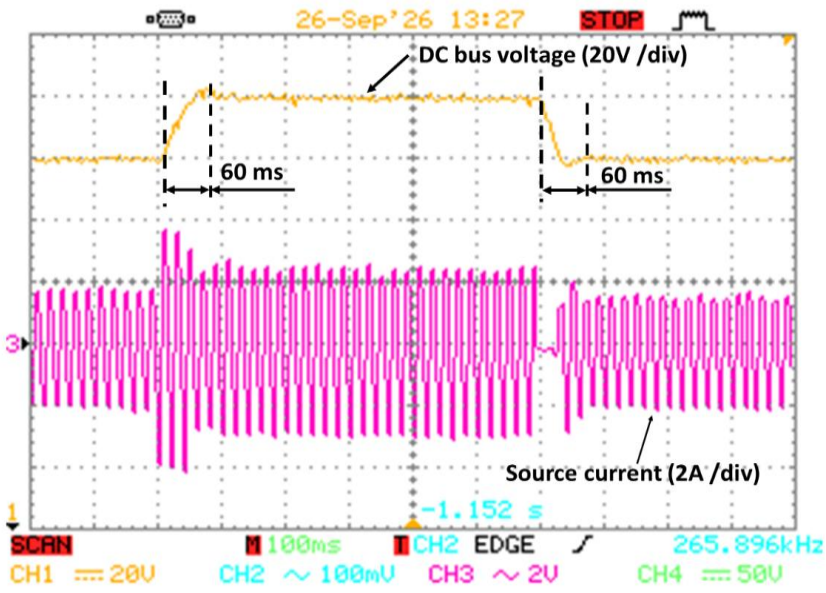

Figure 18. Experimental transient response of the FOPI-controlled PFC converter for successive DC-link voltage reference steps from 120 V to 140 V and from 140 V back to 120 V.

6.3.2.2 A resistive load step change

Figure 19 illustrates the experimental load-transient performance of the FOPI-controlled PFC converter subjected to a load step from 150 Ω to 100 Ω and back to 150 Ω. Following the load transitions, the DC-link voltage undergoes a small deviation of 2 V (undershoot/overshoot) with a rapid recovery time of roughly 60 ms. Meanwhile, the supply current adapts dynamically, confirming the fast transient tracking and stability of the proposed control scheme.

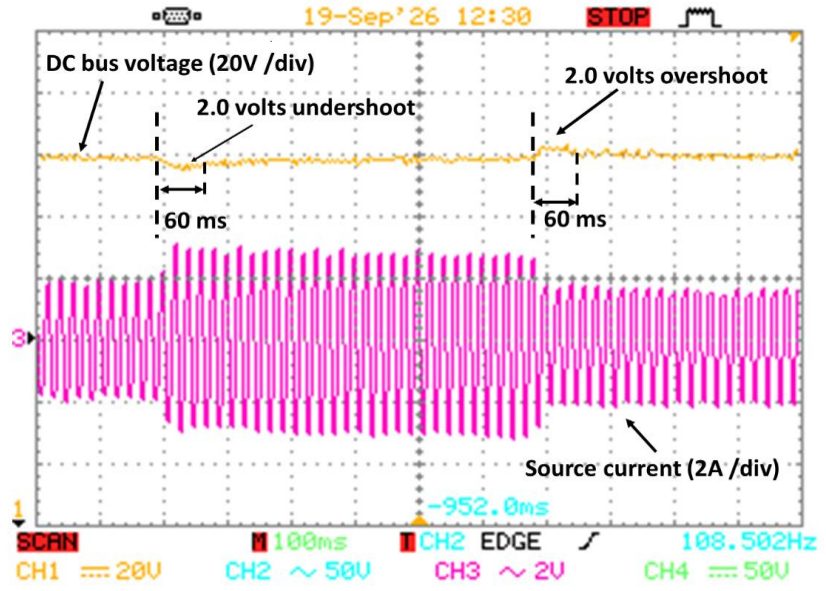

Figure 19. Experimental load-transient response of the FOPI-controlled PFC converter for load resistance changes from 150 Ω to 100 Ω and back to 150 Ω.

6.4 Comparative Discussion of Experimental Results

The experimental comparison of steady-state and dynamic performance for three operating conditions, namely without PFC, with classical PI-controlled PFC, and with the proposed FOPI-controlled PFC, is summarized in Table 5.

Table 5. Experimental comparison of steady-state and dynamic performance under three operating conditions: without PFC, with classical PI-controlled PFC, and with the proposed FOPI-controlled PFC.

	Performance Metric	Without PFC	Classical PI-Controlled PFC	FOPI-Controlled PFC	Improvement (FOPI vs. PI)
Steady-State Performance	Power Factor (PF)	0.743	0.998	0.997	Comparable (both near-unity)
	Displacement Power Factor (DPF)	0.992	0.999	0.999	Comparable
	Current THD (%)	86.3%	3.4%	4.3%	Slightly higher but < 5%
	Voltage THD (%)	5.5%	3.4%	3.4%	Comparable
	Phase Shift (°)	7°	2°	3°	Comparable
	Reactive Power (VAR)	68.0	7.9	8.7	Comparable
DC Bus Voltage Step (120V↔140V)	Settling Time (ms)	N/A	~200 ms	~60 ms	70% reduction (3.3× faster)
	Overshoot/Undershoot	N/A	Negligible	Negligible	Comparable
	Source Current Transient	N/A	Minor spikes	Minor spikes	Comparable
Resistive Load Step(150Ω↔100 Ω)	Settling Time (ms)	N/A	~300 ms	~60 ms	80% reduction (5× faster)
	DC Bus Undershoot/Overshoot (V)	N/A	8 V	2 V	75% reduction
	Source Current Transient	N/A	Minor spikes	Minor spikes	Comparable

7. Results and Discussion

The comparison between simulation and experimental results, presented in Tables 1 and 2, demonstrates excellent agreement for both the classical PI and optimized FOPI controllers, validating the accuracy of the simulation model and the practical feasibility of the proposed control strategy. In terms of steady-state performance, both simulation and experiment confirm that the controllers achieve near-unity power factor and current THD well below the 5% IEEE 519 limit. Small discrepancies, such as the THD of 3.02% in simulation versus 3.4% in experiment for the PI controller, are attributable to measurement noise, component tolerances, and other practical non-idealities. Regarding the DC bus voltage step response, the simulation predicted a settling time of approximately 200 ms for the PI controller and 50 ms for the FOPI controller; the experimental results confirm these values at approximately 200 ms and 60 ms, respectively, demonstrating the FOPI controller's superior reference tracking capability. Under load step conditions, the simulation predicted an 8 V undershoot for the PI controller and negligible deviation for the FOPI controller. The experimental results confirm the 8 V undershoot for PI and show only a 2 V deviation for FOPI, which is slightly higher than the simulation prediction but still significantly better than the PI controller. Overall, the close correlation between simulation and experimental results confirms the validity of the APSO-based FOPI controller design and its practical effectiveness in improving both steady-state power quality and dynamic response in Boost PFC applications.

8. Conclusions

This paper presented the design, Adaptive Particle Swarm Optimization (APSO)-based optimization, and experimental validation of a fractional-order PI (FOPI) controller for a single-phase AC–DC boost PFC converter. The FOPI controller introduces the fractional-order parameter λ as an additional tuning variable, while the Oustaloup approximation enables its practical digital implementation. The controller parameters Kp , Ki , and λ were optimized using an APSO-ITAE-based approach with adaptive PSO coefficients and a composite objective function centered on the ITAE criterion to improve tracking performance while limiting overshoot and control effort.

Simulation and experimental results were conducted under steady-state and transient operating conditions. Both the conventional PI and optimized FOPI controllers achieved near-unity power factor and input-current THD below the 5% IEEE 519 limit. The experimental results also showed good agreement with the simulation results. In particular, the FOPI controller reduced the DC-link voltage settling time from approximately 200 ms for the PI controller to about 60 ms experimentally, compared with approximately 50 ms in simulation. Under load variations, the FOPI controller limited the voltage deviation to approximately 2 V experimentally, compared with an 8 V deviation for the conventional PI controller.

Overall, the results demonstrate that the optimized FOPI controller provides improved dynamic voltage regulation while maintaining satisfactory steady-state power quality, confirming its practical suitability for single-phase boost PFC applications.

9. Funding Declaration

The authors declare that this research received no external funding. No financial support was received from any funding agency, public, commercial, or non-profit organisation.

10. Data Availability' section

All data are included in the article. No additional data are available beyond those presented in the manuscript.

REFERENCES

1. Rashid, M.H., Ed. Power Electronics Handbook, 5th ed.; Butterworth-Heinemann: Oxford, UK, 2024.
2. Singh, B.; Singh, B.N.; Chandra, A.; Al-Haddad, K.; Pandey, A.; Kothari, D.P. A review of single-phase improved power quality AC-DC converters. IEEE Transactions on Industrial Electronics 2003, 50, 962–981. https://doi.org/10.1109/TIE.2003.817609.
3. Mohan, N.; Undeland, T.M.; Robbins, W.P. Power Electronics: Converters, Applications, and Design, 3rd ed.; John Wiley & Sons: Hoboken, NJ, USA, 2003.
4. IEEE. IEEE Standard for Harmonic Control in Electric Power Systems; IEEE Std 519-2022 (Revision of IEEE Std 519-2014); IEEE: New York, NY, USA, 2022; pp. 1–31. https://doi.org/10.1109/IEEESTD.2022.9805001.
5. IEC 61000-3-2, "Limits for harmonic current emissions (equipment input current ≤ 16 A per phase)," 2018
6. ON Semiconductor. Power Factor Correction (PFC) Handbook: Choosing the Right Power Factor Controller Solution; HBD853/D Rev. 5; ON Semiconductor: Denver, CO, USA, 2011.
7. Moschopoulos, G. DC-DC Converter Topologies: Basic to Advanced; Wiley-IEEE Press: Hoboken, NJ, USA, 2024; pp. 1–464.
8. Erickson, R.W.; Maksimović, D. Fundamentals of Power Electronics, 3rd ed.; Springer: New York, NY, USA, 2020.
9. Kazimierczuk, M.K.; Ayachit, A.; Saini, D. Average Current-Mode Control of DC-DC Power Converters; John Wiley & Sons: Hoboken, NJ, USA, 2022; pp. 1–450. https://doi.org/10.1002/9781119525592.
10. A. Tepljakov, *Fractional-Order Modeling and Control of Dynamic Systems*. Springer Cham, 2017, doi: 10.1007/978-3-319-52950-9.

11. Gutiérrez, Ricardo Enrique, Rosário, João Maurício, Tenreiro Machado, José, Fractional Order Calculus: Basic Concepts and Engineering Applications, Mathematical Problems in Engineering, 2010, 375858, 19 pages, 2010. https://doi.org/10.1155/2010/375858.
12. Monje, C.A.; Chen, Y.; Vinagre, B.M.; Xue, D.; Feliu-Batlle, V. Fractional-Order Systems and Controls: Fundamentals and Applications; Springer: Berlin, Germany, 2010. https://doi.org/10.1007/978-1-84996-335-0.
13. Scherer, R.; Kalla, S.L.; Tang, Y.; Huang, J. The Grünwald–Letnikov Method for Fractional Differential Equations. *Comput. Math. Appl.* **2011**, 62, 902–917. https://doi.org/10.1016/j.camwa.2011.03.054.
14. Oustaloup, A., et al. "Frequency-band complex non integer differentiator: Characterization and synthesis." IEEE Trans. Circuits Syst. I, 2000.
15. Oustaloup A La commande crone: commande robuste dordre non entier. 1991, Hermès, Paris.
16. Reddy, A.S., Reddy, G.N. Novel applications of oustaloup recursive approximation and modified oustaloup recursive approximation methods in linear fractional order control design. Int. J. Dynam. Control 12, 2236–2246 (2024). https://doi.org/10.1007/s40435-023-01351-x.
17. Wendimu, A.A.; Matušů, R.; Shaikh, I.; Wolde, M.K.; Roba, M.T.; Yareshe, F.T. A Unified Comparative Framework for Fractional-Order Operator Approximation with Pareto-Based Analysis. Fractal Fract. 2026, 10, 321. https://doi.org/10.3390/fractalfract10050321
18. B. Song, L. Xu and X. Lu, "A comparative study on Tustin rule based discretization methods for fractional order differentiator," 2014 4th IEEE International Conference on Information Science and Technology, Shenzhen, China, 2014, pp. 515-518, doi: 10.1109/ICIST.2014.6920529.
19. Adhikary, B.; Swarnakar, J. A Novel Approach towards Discrete-Time Realization of Fractional-Order Proportional Integral Controller. Commun. Nonlinear Sci. Numer. Simul. 2026, 152, 109322. https://doi.org/10.1016/j.cnsns.2025.109322.
20. J. Kennedy and R. Eberhart, "Particle swarm optimization," *Proceedings of ICNN'95 - International Conference on Neural Networks*, Perth, WA, Australia, 1995, pp. 1942-1948 vol.4, doi: 10.1109/ICNN.1995.488968.
21. Eberhart and Yuhui Shi, "Particle swarm optimization: developments, applications and resources," *Proceedings of the 2001 Congress on Evolutionary Computation (IEEE Cat. No.01TH8546)*, Seoul, Korea (South), 2001, pp. 81-86 vol. 1, doi: 10.1109/CEC.2001.934374.
22. Ballouti, A.; Bentata, K.; Amroune, S.; Saada, K.; Boumaaza, M. FPGA-in-the-Loop Validation of a Systematic-Sequencing Adaptive Particle Swarm Optimization Algorithm for Photovoltaic Under Partial Shading. *Energies* 2026, *19*, 3896. https://doi.org/10.3390/en19163896
23. Idir, A.; Kidouche, M.; Bensafia, Y.; Khettab, K.; Tadjer, S.A. Speed control of DC motor using PID and FOPID controllers based on differential evolution and PSO. Int. J. Intell. Eng. Syst. 2018, 20, 21.
24. D. Sinha, M. D. Mahapatra, S. Pal, S. Majumder, S. Bhattacharya, and C. Bandyopadhyay, "Adaptation of fractional-order PI controller for a variable input interleaved DC–DC boost converter using particle swarm optimization with parametric variation," IFAC Journal of Systems and Control, vol. 32, Art. no. 100301, 2025, doi: 10.1016/j.ifacsc.2025.100301.
25. Aliskan, I. The Fractional-Order Proportional-Integral-Derivative Controller Tuned with Hybrid Particle Swarm Optimization-Artificial Bee Colony Algorithm for Boost Converters: An Experimental Study. Arabian Journal for Science and Engineering 2026, 51, 19601. https://doi.org/10.1007/s13369-026-11423-7
26. Elyaalaoui, Kamal, Labbadi, Moussa, Ouassaid, Mohammed, Cherkaoui, Mohamed, Optimal Fractional Order Based on Fuzzy Control Scheme for Wind Farm Voltage Control with Reactive Power Compensation, Mathematical Problems in Engineering, 2021, 5559242, 12 pages, 2021. https://doi.org/10.1155/2021/5559242
27. Idir, A.; Canale, L.; Bensafia, Y.; Khettab, K. Design and Robust Performance Analysis of Low-Order Approximation of Fractional PID Controller Based on an IABC Algorithm for an Automatic Voltage Regulator System. Energies 2022, *15*, 8973. https://doi.org/10.3390/en15238973
28. Sahib, M. A novel optimal PID plus second order derivative controller for AVR system. Eng. Sci. Technol. Int. J. 2014, 18, 1–13.
29. Bensafia, Y.; Khettab, K.; Idir, A. An Improved Robust Fractionalized PID Controller for a Class of Fractional-Order Systems with Measurement Noise. Int. J. Intell. Eng. Syst. 2018, 11, 200–207.

30. Ballouti, A.; Belhaouchet, N.; Benhamadouche, A.D. FPGA Implementation of Fixed-Point Model for a Single-Phase AC-DC Converter with Unity Power Factor. Journal Européen des Systèmes Automatisés 2022, 55, 181–187. https://doi.org/10.18280/jesa.550204